ISSN 1070-3284, Russian Journal of Coordination Chemistry, 2021, Vol. 47, No. 1, pp. 66–74. © Pleiades Publishing, Ltd., 2021.

Preparation, Two-Photon Absorption, and Bioimaging Application of a Curcumin-Based Copper(II) Complex

G. F. Si[a], Y. Zhou[b], J. F. Wang[a], G. Y. Xu[c, *], and S. S. Zhou[a, c, **]

[a] *Department of Pharmacy, Anhui University of Chinese Medicine, Hefei, 230012 P.R. China*

[b] *Qlu School of Medicine, Shandong University, Jinan, 502100 P.R. China*

[c] *Institutes of Physical Science and Information Technology, Anhui University, Hefei, 230601 P.R. China*

**e-mail: gyxu@mail.ustc.edu.cn*

***e-mail: zhouss_321@126.com*

Received September 5, 2019; revised November 3, 2019; accepted November 28, 2019

Abstract—A new multi-branched model Cu(II) complex based on curcumin, namely CuL_2(I) (HL = (1*E*,4*Z*,6*E*)-1,7-bis(4-(4-bromobutoxy)-3-methoxyphenyl)-5-hydroxyhepta-1,4,6-trien-3-one, $C_{29}H_{34}O_6Br_2$), was prepared and its two-photon absorption (TPA) properties were described in the femtosecond regime. The experimental results showed that complex **I** exhibited relatively strong and wide-dispersed two-photon activities in the near-infrared (NIR) regime and the calculated TPA cross section of complex **I** was as high as 872 GM (1 GM = 10^{-50} cm^4 s $photon^{-1}$) in DMF. Additionally, complex **I** revealed its potential application as a biological fluorescent probe due to its good photo-physical properties and low cytotoxicity, as well as excellent stability and specificity for optical imaging of tumors. Complex **I** was characterized by single crystal X-ray diffraction too (CIF file CCDC no. 1412447).

Keywords: curcumin, two-photon absorption, single crystal X-ray diffraction, bioimaging

DOI: 10.1134/S1070328420110081

INTRODUCTION

In the past decades, materials with large two-photon absorption (TPA) cross section have attracted significant attention because of the very promising TPA-based applications [1–3]. One of the most significant applications of TPA materials is biological imaging in living cells and tissues relying on the development of the two-photon microscopy (TPM) technique, which not only provides a number of advantages in biological imaging, e.g. reduced phototoxicity, increased penetration depth, and negligible background fluorescence, but also monitors and records molecular spatiotemporal distribution, cellular biochemistry processes and even detects earlier diseases [4–6]. Thus, considerable research efforts have been devoted to the development of new chromophores with large TPA cross section for the use in biological imaging, such as polymers, multi-branched organic molecules, semiconductors or nanoparticles, and metal complexes [7–9].

In current research in the field of TPA materials, well-accepted design approach to achieve large cross section is generally based on the introduction of an electron donor and acceptor to the ends of a π-conjugated system according to Albota [10] and Reinhardt [11]. Based on their design strategy, a series of chromophores were developed with the structures of donor-π-donor (D-π-D) type,donor-π-acceptor (D-π-A) type and acceptor-π-acceptor (A-π-A) type [12–14]. On the other hand, it has been reported that the TPA cross sections of multi-branched molecules could be strongly enhanced compared with those of their one-branched counterparts [15, 16]. The theoretical study predicted that the TPA cross section of the metal complex should be much higher than that of the corresponding ligand [17]. For example, a Cu(I) complex $[Cu_4I_4L_4]$, led to great increase of the TPA cross section compared with its ligand (L = (*E*)-(4-diethylanilino-styryl)pyridine] [18]. However, the syntheses of D-π-D type, D-π-A type, A-π-A type or multi-branched compounds, as well as metal complexes, were suffered from the complicated procedures and low-yielding, which limited their practical application. Structural stable TPA dyes exhibiting large cross section and also emitting strong fluorescence *via* direct two-photon excitation at a longer wavelength are still few at present.

Curcumin 1,7-bis-(4-hydroxy-3-methoxyphenyl)-1,6-heptadiene-3,5-dione, which is obtained from the rhizome of *Curcuma longa* Linn, is a natural phenolic pigment with low toxicity and good stability and also a common ingredient used in cosmetics, spices and traditional Chinese medicines in Asian countries [19]. The compound and its derivatives have been reported to possess good optical and electrical properties

because of a highly π-electron delocalized system and symmetric structure [20, 21].

In searching highly efficient TPA materials based on the above strategies, in this article, we report a novel multi-branched Cu(II) complex based on curcumin with a D-π-D structure, namely CuL_2 (**I**) (HL = (1*E*,4*Z*,6*E*)-1,7-bis(4-(4-bromobutoxy)-3-methoxyphenyl)-5-hydroxyhepta- 1,4,6-trien-3-one, $C_{29}H_{34}O_6Br_2$). Simultaneously, the photo-physical properties and cytotoxicity of complex **I** were also investigated. In addition, the application of complex **I** as a fluorescent probe in vitro and in vivo for the biological imaging was also studied. The synthetic route of the Cu(II) complex is presented in Scheme 1.

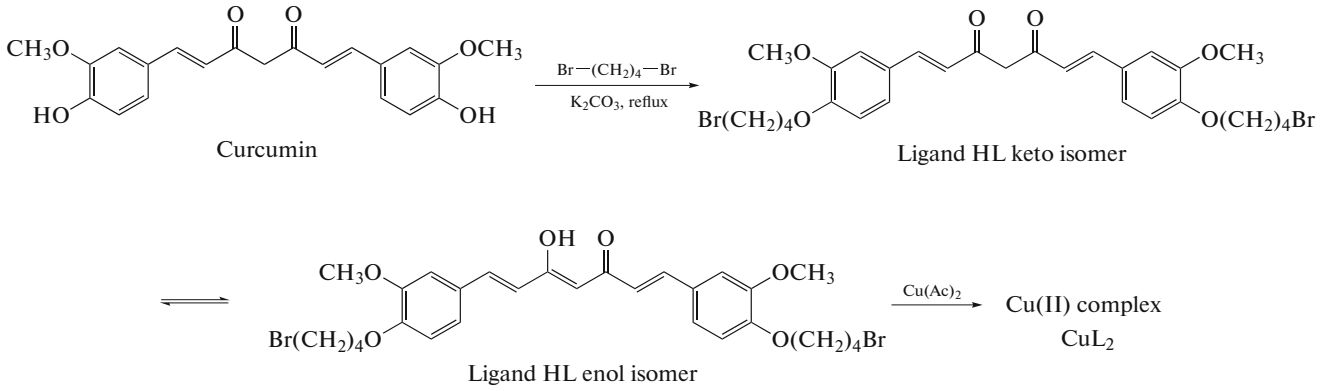

Scheme 1.

EXPERIMENTAL

Materials and methods. All chemicals were available commercially and every solvent was purified by conventional methods before use. Double distilled water was used throughout all experiments. All compounds were at first dissolved in DMSO to 2 mM, and then diluted by phosphate buffer solution (PBS, pH 7.2, Gibco) to different concentration. Each solution used for photo-physical properties is freshly prepared and kept in the dark before measurement.

Melting points were determined on WRS-2 (Shanghai China). Fourier transform infrared (FTIR) spectra were recorded on SHIMADZU IR Prestige-21 spectrophotometer with samples prepared as KBr (spectrum pure) pellets. ^{1}H NMR spectrum was performed on a Bruker AV^{II}400 spectrometer with tetramethyl silane ($Si(CH_3)_4$) as the internal standard. The mass spectrum was obtained on FINNIGAN LCQ Advantage MAX LC/MS (Thermo Finnigan, American). Elemental analyses were carried out with a Perkin-Elmer 240C analyzer.

The UV-Vis absorption spectra were recorded on a SPECORD S600 spectrophotometer. The one-photon excited fluorescence (OPEF) spectra were performed using a Hitachi F-7000 fluorescence spectrophotometer. The one-photon absorption (OPA) and OPEF spectra of HL and CuL_2 were measured in four organic solvents of different polarities at a concentration of 1.0×10^{-5} mol/L. The quartz cuvettes used had a 1 cm path length. The fluorescence quantum yields (Φ) of the compounds were measured according to literature [14]. The two-photon induced fluorescence spectra were recorded with a certain laser beam from a mode-locked Ti:sapphire laser (Coherent Mira 900 F) as the pump source with a pulse duration of 200 fs, a repetition rate of 76 MHz, and a single-scan streak camera (Hamamatsu Model C5680-01) together with a monochromator as the recorder. The photostability of complex **I** was performed by a mercury lamp of 50 W with continuous irradiation of 2 h. ICG and LTG molecules (two commercial dyes) were used for comparison.

Synthesis of HL. Curcumin (1.8 g, 5 mmol) was added to DMF solution (30 mL) containing anhydrous potassium carbonate (1.30 g, 10 mmol) and heated at 80°C for 30 min, then redistilled 1,4-dibromobutane (2.2 g, 10 mmol) and a small quantity of potassium iodide were added into the reaction system. The mixture was refluxed for about 6 h at 80°C and monitored by thin-layer chromatography (TLC). After the completion of the reaction, the resultant mixture solution was added into 50 mL of cold water under violent stirring. The yellow solid was obtained by filtration. The crude product was purified by column chromatography over silica gel eluting with ethyl acetate–petroleum ether mixture (5 : 6, v/v) as the eluent to get the pale yellow microcrystal. The yield was 52%. m.p. 124–126°C.

For $C_{29}H_{34}O_6Br_2$		
Anal. calcd., %	C, 54.56	H, 5.37
Found, %	C, 54.73	H, 5.56

Table 1. The crystallographic data and structure refinement for CuL_2

Parameter	Value
Formula weight	1338.28
Temperature, K	296(2)
Crystal system	Monoclinic
Space group	$P2_1/n$
a, Å	14.098(2)
b, Å	8.4699(15)
c, Å	25.151(5)
β, deg	100.580(2)
Volume, Å^3	2952.3(10)
Z	2
ρ_{calcd}, g cm^{-3}	1.505
μ, mm^{-1}	3.135
F(000)	1358
$\theta_{min}-\theta_{max}$, deg	2.54–26.30
Reflections collected	22149
Reflections unique	6094
R_{int}	0.0435
Data/restraints/parameters	6094/14/342
Final R indices ($I > 2\sigma(I)$)	$R_1 = 0.0891$, $wR_2 = 0.2676$
R indices (all data)	$R_1 = 0.1436$, $wR_2 = 0.3114$
GOOF on F^2	1.043
$\Delta\rho_{max}/\Delta\rho_{min}$, e Å^{-3}	2.23/–1.17

^{1}H NMR (DMSO; 400 MHz; δ, ppm): 1.51–1.59 (s., 9H, CH_3), 2.01–2.24 (m., 6H, OCH_2), 3.48–3.55 (s., 6H, OCH_3), 4.09–4.16 (m., 6H, CH_2), 5.11 (s., 1H, COC*H*CO), 7.08–7.23 (m., 6H, Ar–*H*), 7.56–7.63 (m., 4H, C*H*). MS ESI (*m/z*): 638.38 ([M+H]$^+$, 100).

Synthesis of CuL_2 (I). HL (1.3 g, 3.0 mmol) was dissolved in ethanol (30 mL), then solid sodium hydroxide (0.12 g, 3.1 mmol) and a solution of $Cu(OAc)_2$ (0.35 g, 2.0 mmol) in ethanol (20 mL) were added into the above solution sequentially at room temperature. The reaction mixture was stirred at 80ºC for 5 h. After cooling to room temperature, yellow green solid was filtered, washed with water and ethanol, respectively, and then dried under vacuum at 50°C. The yield was 62%. m.p. > 250°C.

For $C_{58}H_{66}O_{12}Br_4Cu$

Anal. calcd., %	C, 52.05	H, 4.97	Cu, 4.74
Found, %	C, 52.35	H, 4.68	Cu, 4.52

FTIR (KBr; ν, cm^{-1}): 2.979 (CH_3), 1.623 (C=O), 1.510 (C=C), 1.598, 1.577, 1.477 (Ar), 1.257 (=CH), 543 (Cu–O).

Single-crystal X-ray diffraction. The structure data of complex **I** were carried out on a Seimens Smart 1000 CCD diffractometer equipped with a graphite crystal monochromator situated in the incident beam for data collection at room temperature. The determination of unit cell parameters and data collections were performed with MoK_α radiation (λ = 0.71073 Å). Unit cell dimensions were obtained with least-square refinements, and all structures were solved by the direct method as SHELXL-97 [22]. The final refinement was performed by full-matrix least-square methods with anisotropic thermal parameters for non-hydrogen atoms on F^2. The hydrogen atoms were added theoretically and riding on the concerned atoms. The crystallographic data for complex **I** are presented in Table 1, selected bond lengths and angles are shown in Table 2.

Supplementary material for structures HL and **I** has been deposited with the Cambridge Crystallographic Data Centre (CCDC nos. 896630 and

Table 2. Selected bond length (Å) and angle (deg) of complex CuL_2

Bond	*d*, Å	Angle	ω, deg
Cu(1)–O(3)	1.899(4)	O(3)Cu(1)O(3)	180.0
Cu(1)–O(4)	1.901(4)	O(3)Cu(1)O(4)	86.96(18)
C(9)–C(12)	1.438(8)	O(3)Cu(1)O(4)	93.04(18)
C(12)–C(13)	1.346(8)	O(4)Cu(1)O(4)	180.0(2)
C(13)–C(14)	1.462(8)	C(8)C(9)C(12)	123.3(5)
C(14)–C(15)	1.371(8)	C(10)C(9)C(12)	119.2(6)
C(15)–C(16)	1.392(8)	C(10)C(9)C(8)	117.5(5)
C(16)–C(17)	1.478(8)	C(18)C(19)C(24	124.7(6)
C(17)–C(18)	1.324(8)	C(20)C(19)C(18)	117.3(6)
C(18)–C(19)	1.458(8)	C(24)C(19)C(20)	118.0(6)

1412447, respectively; deposit@ccdc.cam.ac.uk or http://www.ccdc.cam.ac.uk/conts/retrieving.html).

Cell culture and cytotoxicity assay. Cytotoxicity is a potential side effect of the dye that must be controlled when dealing with living cells or tissues. To ascertain the cytotoxic effect of HL and CuL_2 treatment over a 24 h period, the 5-dimethylthiazol-2-yl-2,5-diphenyltetrazolium bromide (MTT) assay was performed. Human breast carcinoma (MCF-**7**) cells were trypsinized and plated to 70% confluence in 96-well plates 24 h before treatment. MCF-7 cells were seeded into a 96-well culture plate at about 2.0×10^5 cell/well. 50 mL of the sample solution diluted with DMEM at different concentrations was added to each well, respectively. The cells were cultivated for 24 h at 37°C, 5% CO_2 and 95% air, followed by the addition of 50 mL MTT solution (5 mg/mL) to each well and incubated for an addition 2 h (37°C, 5% CO_2 and 95% air). Then, DMEM was removed, the cells were dissolved in DMSO (150 mL/well), the absorbance of each cell was determined by UV spectrometer at 540 nm. The percentage of cell viabilities was calculated by the following equation: cell viability = $(OD_{treated}/OD_{control}) \times 100\%$, where $OD_{treated}$ was obtained in the presence of sample at various concentration, $OD_{control}$ was obtained from the incubation medium. Three independent trials were conducted, and the percentage of viable cells was calculated averagely relative to untreated cells.

Two-photon fluorescence image. Cells were seeded in 6 well plates at a density of 5×10^4 cells per well and grown for 96 h. For live cell imaging MCF-7 cells were incubated with the Cu(II) complex (10% PBS/90% cell media) at concentration of 10 μM and maintained at 37ºC in an atmosphere of 5% CO_2 and 95% air for incubation time of 0.5 h. The cells were then washed with PBS (3 × 3 mL per well), and 3 mL of PBS was added to each well. MCF-7 cells were luminescently imaged on a Zeiss LSM 510 META upright confocal laser scanning microscope using magnification 40× and 100× water-dipping lenses for monolayer cultures. Image data acquisition and processing was performed using Zeiss LSM Image Browser, Zeiss LSM Image Expert and Image J. Excitation energy of 780 nm was used, and the fluorescence emission was measured at 550–650 nm.

Animal experiments and in vivo cell imaging. Normal Kunming mice were purchased from Animal Laboratory of China Pharmaceutical University (Nanjing, China). All animal experiments were performed in compliance with the Animal Management Rules of the Ministry of Health of the People's Republic of China. Anesthetized mice were injected with HepG2 tumor cell suspension (about 4×10^5 cells in 0.2 mL of PBS) into the left flank area of the nude mice. After 15 days of tumor cell incubation, the tumor grew up to a diameter of about 0.2 cm, then, 0.5 mL of CuL_2 in PBS (10.0 μM) was administered into each tumor-bearing mouse through tail vein injection. After injection of the target compound probe (2 h), two-photon fluorescence imaging was measured by the IVIS Lumina system (Xenogen Co., Alameda, CA, USA).

RESULTS AND DISCUSSION

The structures of HL[1] and CuL_2 (Fig. 1) were further confirmed by single-crystal X-ray diffraction. Single crystals of two compounds suitable for X-ray crystallography analysis were grown from ethyl acetate/ethanol (6 : 1) and DMF/THF (5 : 1 v/v), respectively. As shown in Fig. 1, each copper(II) center has a square planar coordinated sphere surrounded by four oxygen atoms from two chelating β-diketone ligands in their enol form. The Cu(1)–O(3) and Cu(1)–O(4) bond lengths are 1.899(4) and 1.901(4) Å (Table 2), respectively, which are smaller than those in other copper diketonate complexes [19]. The O(3)Cu(1)O(4) bond angles are 86.96(18)° and 93.04(18)°, respectively, and the sum is 180°, revealing that the Cu(II) center adopts a square planar geome-

[1] See the supplement materials.

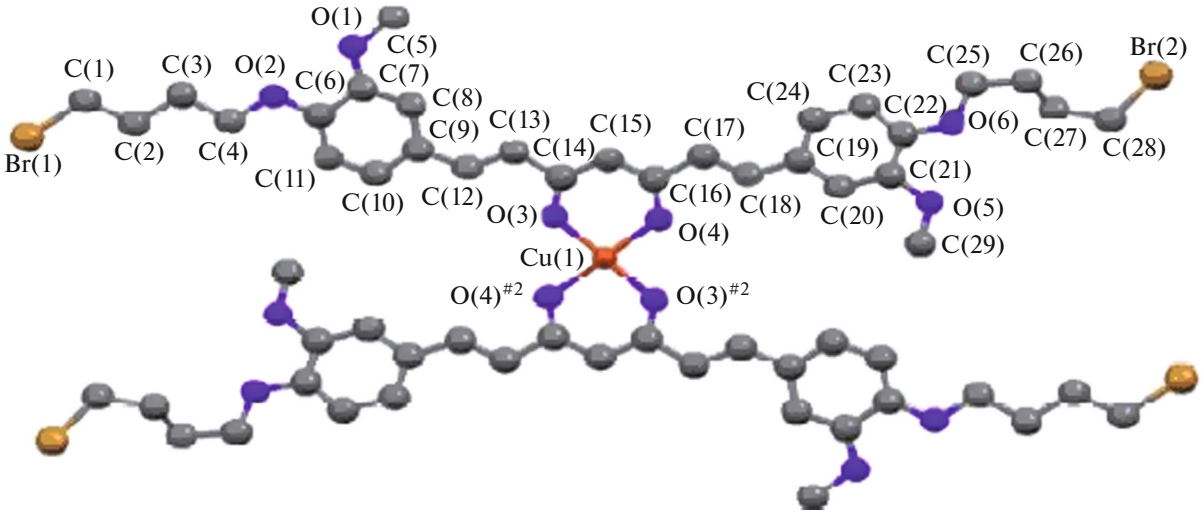

Fig. 1. ORTEP structure of CuL_2 with 50% probability (all hydrogen atoms are omitted for clarity).

try. It can be seen from Table 2 that the bond lengths are intermediate, such as C(9)–C(12) 1.438(8), C(12)–C(13) 1.346(8), C(13)–C(14) 1.462(8), C(14)–C(15) 1.371(8), C(15)–C(16) 1.392(8), C(16)–C(17) 1.478(8), C(17)–C(18) 1.324(8), and C(18)–C(19) 1.458(8) Å, suggesting that there is a highly π-electron delocalized system in the metal complex molecule. The sum of the three CCC bond angles is 360°, which take carbon atom (C(9)) as center (C(8)C(9)C(12) 123.3(5)°, C(10)C(9)C(12) 119.2(6)°, C(10)C(9)C(8) 117.5(5)°). This result demonstrates that the carbon atom (C(12)) is practically coplanar with the benzene ring. Additionally, the deviation angle between benzene ring and the coordination plane composed of one Cu(II) atom and four oxygen atoms is 6.52°, and the deviation angle between two benzene rings in each ligand is 9.26°. The structural character indicates the good coplanarity and large π-conjugated system in the complex, which is necessary for large TPA cross section [17, 23]. The packing diagram of the complex shows that the adjacent molecules are stacked through two types of π–π interactions along the *a* and *c* axes with the short distances of 3.468 and 3.687 Å, respectively.

The photo-physical properties of HL and CuL_2 were summarized in Table 3 and Figs. 2a–2e. The linear absorption and OPEF spectra of the two compounds were measured in four solvents of different polarity at a concentration of $c = 1.0 \times 10^{-5}$ mol/L, in which the solvent influence was not included. From the linear absorption curves of the two compounds in DMF, shown in Fig. 2a, we observed that absorption maximum located at 356 nm for HL (with the corresponding mole absorption coefficient $\varepsilon = 3.42 \times 10^4$ cm^{-1} M^{-1}) and 358 nm for CuL_2 ($\varepsilon = 3.77 \times 10^4$ cm^{-1} M^{-1}), corresponding to the n–π* transition of the compounds. The shorter wavelength at 262 nm for HL ($\varepsilon = 1.7 \times 10^4$ cm^{-1} M^{-1}) and 263 nm for CuL_2 ($\varepsilon = 3.8 \times 10^4$ cm^{-1} M^{-1}) originated from the π–π* transition of oxygen atom and benzene ring [24]. The ε value of CuL_2 was significantly higher than that of HL, which might be due to the extension of π-conjugation and coordination of metal ion with its corresponding ligand [25].

Figure 2b is the OPEF spectra of HL and CuL_2 in DMF with the same concentration as that of the linear absorption spectra, the maximum emission wavelengths of HL and CuL_2 are 520 and 525 nm, respectively. From Table 3, one can see that the maximum absorption peaks clearly show a red-shift with the increase of the polarity of the solvent for each compound, which can be explained by the fact that the excited state of these compounds may possess higher polarity than the ground state, since the solvatochromism is associated with the energy level lowering. The increasing dipole-dipole interaction between the solute and solvent leads to the great energy level lowering [25, 26].

The fluorescence quantum yield was performed in solvent following the procedure described by us before [23]. It can be seen from Table 3 that the quantum yield of CuL_2 was significantly higher than that of its corresponding ligand, and upon increasing the solvent polarity, the fluorescence quantum yield exhibited obvious increase.

Figure 2c shows the two-photon fluorescence of two compounds in DMF with a concentration of $c = 1.0 \times 10^{-3}$ mol/L. Comparing the TPEF spectra (Fig. 2c) with their corresponding OPEF spectra (Fig. 2b), we find there are obviously many similarities. Firstly, the TPEF spectrum shape of any of the compounds is similar to the corresponding OPEF spectrum shape. Secondly, the TPEF peak position of

Table 3. The photo-physical properties of HL and CuL_2 in different solvents*

Compound	Solvent	λ_{max}^{abs}, nm	$\varepsilon/10^4$	λ_{max}^{1f}, nm	λ_{max}^{2f}, m	Φ^a	$\Delta\nu^b$	$\sigma_{max}{}^c$
HL	CH_2Cl_2	371		491			6583	425
	EtOH	380	4.13	499		0.18	6280	417
	DMF	356		520	520		6719	374
	DMSO	381	3.82	520		0.31	7009	391
CuL_2	CH_2Cl_2	386		493			5626	1128
	EtOH	391	3.64	500		0.43	5570	1051
	DMF	358		525	521		6309	1036
	DMSO	404	3.42	520		0.54	6519	1042
			4.36			0.22		
			4.13			0.37		
			3.92			0.48		
			3.77			0.64		

* λ_{max}^{abs} and λ_{max}^{1f} represent the maximum wavelength of linear absorption and single-photon fluorescence, respectively. It is filtered through a 0.2 mm Gelman acrodisc CR filter. [a] Quantum yield (Φ) at room temperature was determined with Coumarin ($\Phi = 0.56$ in ethanol) as a reference in DMF. [b] Stokes shift in cm^{-1}. [c] TPA cross section in GM (1 GM = 10^{-50} cm^4 s $photon^{-1}$ $molecule^{-1}$).

two compounds is basically the same sequence of λ (HL) < λ (CuL_2) as the corresponding OPEF peak position. Thirdly, the relative TPEF intensities of these compounds show the same spectral sequence of HL < CuL_2 as those of OPEF. These similarities between TPEF and OPEF indicate that both the emissions for a given compound are from the same excited state, though their initial Frank-Condon states may be different. The difference between TPEF and OPEF is mainly at the excitation process: two-photon absorption vs. single photon absorption [26]. From Table 3, it can be seen that the peak positions of TPEF show red shift compared to those of OPEF, which can be explained by the effect of reabsorption in the high concentration solution [23].

Two-photon fluorescence spectra of complex I in DMF pumped by femtosecond laser pulses at 600 mW through different excitation wavelengths are also presented in Fig. 2e. The excitation wavelengths are in the NIR region (690–860) due to their more extensive π-conjugation and the presence of intramolecular charge transfer (ICT) process [27]. No linear absorption was observed in the range from 500 to 1000 nm, so the emission excited by NIR laser wavelength can be attributed to the TPEF mechanism. The two-photon cross section σ was measured by the method reported based on the comparison of fluorescence intensity (PL) [25], as shown in Fig. 2d. The calculated largest TPA cross section σ of the obtained complex in DMF is 872 GM (1 GM = 10^{-50} cm^4 s $photon^{-1}$) at 780 nm (Fig. 2d), which is about 1.6 times larger than that of the corresponding ligand ($\sigma = 546$ GM), which can be explained by the enlarged coplanarity and the following increased π-electron polarization when the Cu^{2+} cations are coordinated with the ligands, eventually leading to an increase in the TPA cross section values.

To verify the fluorescence stability as a cellular fluorescent probe, the photostability of complex **I** was determined. As exhibited in Fig. 2f, the PL intensities of complex **I** maintained over 80% of the original PL intensity after 2 h of continuous irradiation by a mercury lamp of 50 W. For comparison, ICG and LTG molecules (two commercial dyes) were determined, only less than 15% of original PL intensities were maintained under the same conditions. The results show the superior photostability of complex **I** compared with ICG and LTG, implying its potential application for long-term biomedical imaging.

Figure 3a displays the cell viability of tested MCF-7 cell lines when treated with different concentrations of each compound for 24 h. The results clearly indicated that no obvious cell viability decreased, even when the concentration of the two compounds HL and CuL_2 reached up to 20 μmol/L (two times of the concentration used for bioimaging in our study), the cell viability was still greater than 80%. The low cytotoxicities of the obtained compounds indicate they are suitable for cellular imaging applications.

MCF-7 cells were selected toward complex **I** for biological imaging. MCF-7 cells were cultured and stained with the complex, and then the image was taken after 0.5 h staining (Fig. 3b, left). It can be seen that the complex probe went through the membrane and localized uniformly in the cytoplasm while a few bright spots in the nucleus, implying the cell cytoplasm can be labeled mainly by the obtained complex probe. For comparison, MCF-7 cells were stained with a nuclear dye Hoechst 33342 (a commercially available organic dye) and the image was performed

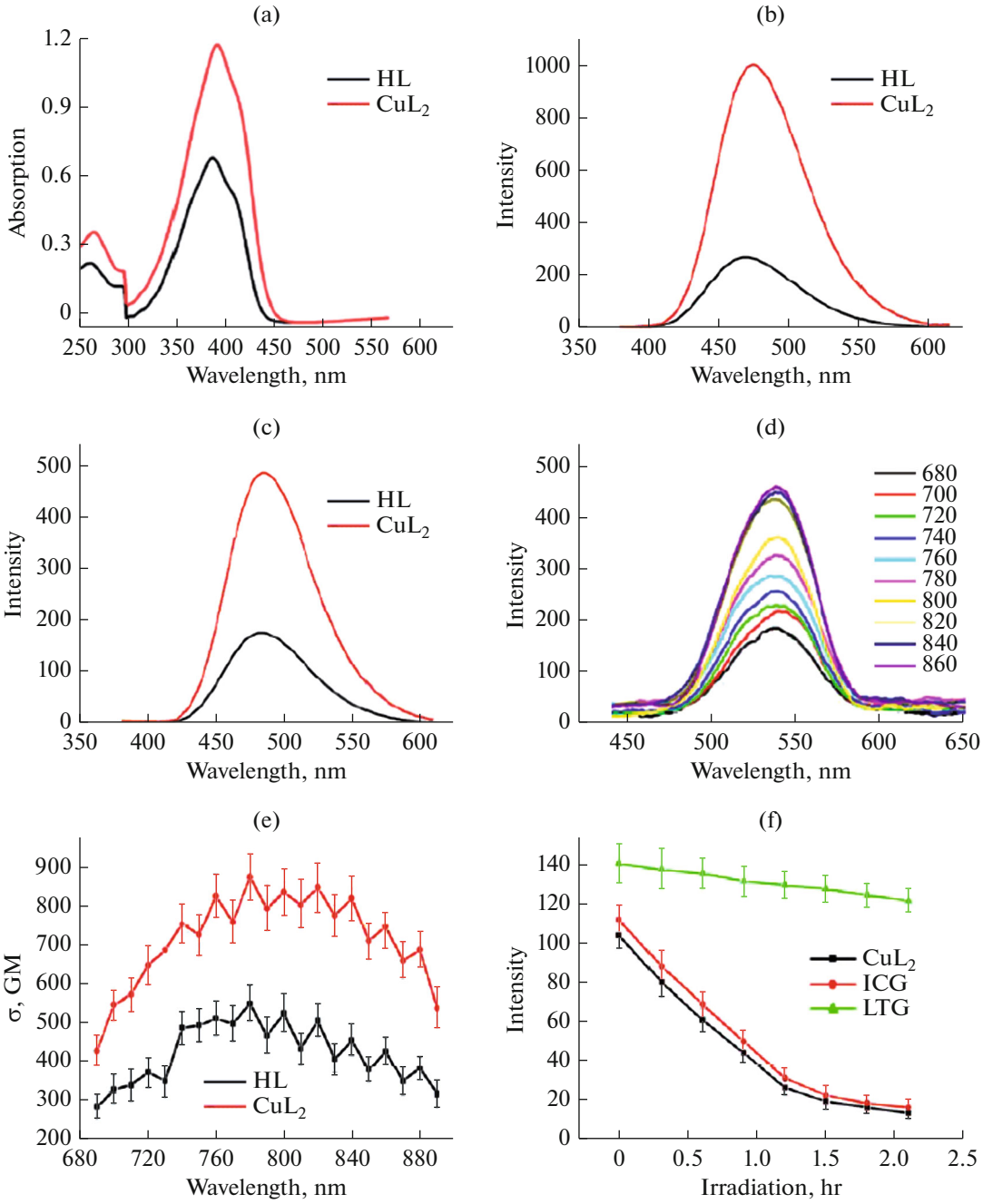

Fig. 2. Linear absorption (a), OPEF (b) and TPEF (c) spectra of HL and complex **I** in DMF; the TPEF spectra of CuL_2 in DMF pumped by femtosecond laser pulses at 600 mW at different excitation wavelengths (d); TPA cross section of the compounds in DMF versus excitation wavelengths of identical energy of 0.380 W (e); fluorescence intensities of CuL_2, ICG and LTG during irradiation time (f).

under the same condition (Fig. 3b, middle). The merged image (Fig. 3b, right) showed that the complex probe emitted bright green fluorescence outside the nuclei and the dye Hoechst 33342 emitted blue fluorescence inside the nuclei.

To validate the feasibility of CuL_2 as a NIR imaging probe, the tumor targeting ability of the complex **I** was carried out with a model of HepG2 liver tumor-bearing mice. Mice images were taken before and after intravenous injection of CuL_2 at 10.0 μM dosage by the IVIS Lumina imaging system in a dark room at specific time intervals. Figure 3c shows the in vivo imaging of complex **I** after injection in living mice. The tumor sites were identifiable within 2 h postinjection of the complex probe. Interestingly, the probe increasingly accumulated in the tumors and the stron-

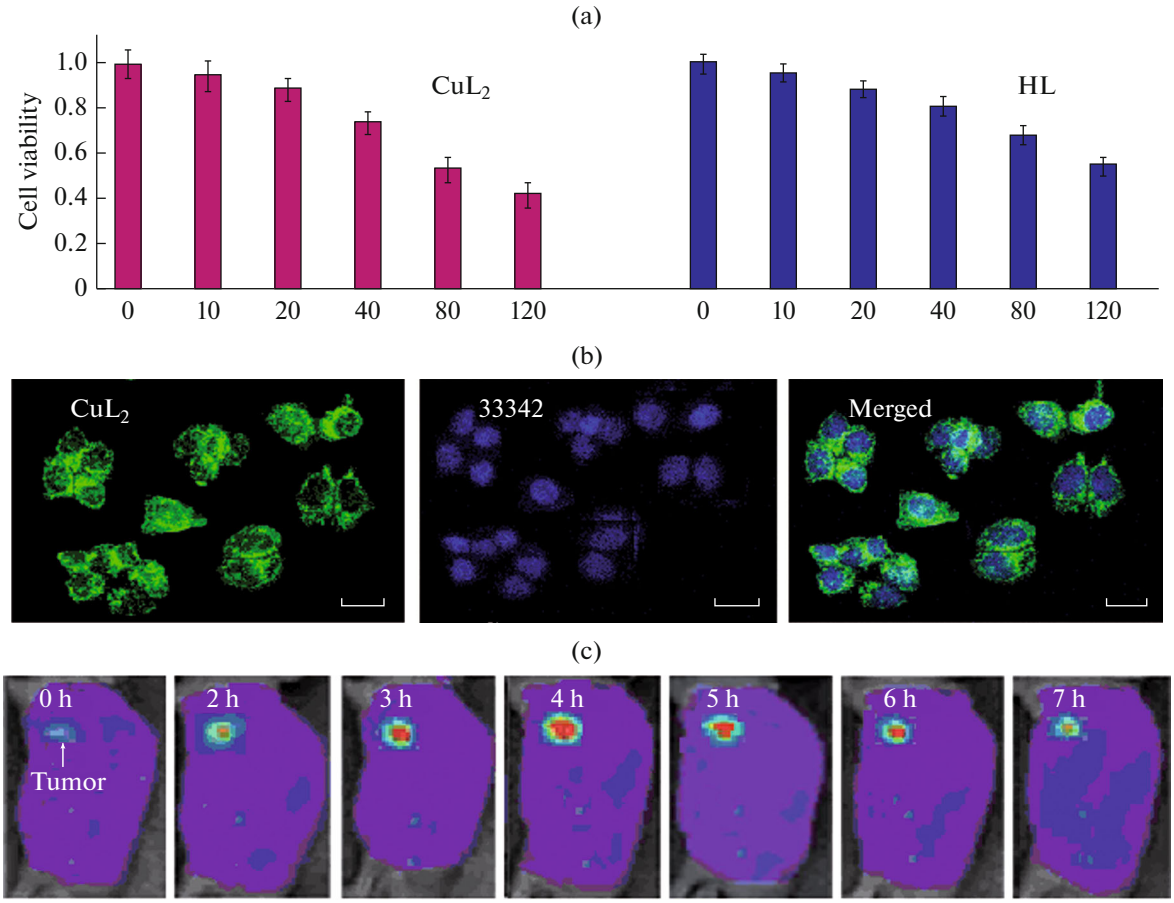

Fig. 3. Cytotoxicity data results of HL and CuL_2 against MCF-7 cell lines (24 h) from the MTT assay (a); fluorescence images of MCF-7 cells incubated and stained for 0.5 h: green (left)—imaging stained with 10 μM of CuL_2, blue (middle)—cell nuclei stained with Hoechst 33342, merged image (right) (all the scale bars represent 10 nm) (b); fluorescence images of nude mice bearing HepG2 tumor at different time after injected with CuL_2 (c).

gest fluorescence signal was detected in the liver tumor of mice 4 h after injection. However, as time goes on, the blue light signal decreases slowly, which may suffer from relatively intense absorption and scattering caused by the animal tissue and body fluids. The signal still can be clearly observed even after 6 h post injection of probe. The in vivo imaging results exhibit the potential applications of the as-prepared compound toward tumor tissues though intense background luminescence or autofluorescence might be encountered.

ACKNOWLEDGMENTS

The authors thank Dr. Fucheng Sheng, Hongxing Liu and Ming Zhang from University of Science and Technology of China for their valuable technical assistance in biological imaging.

FUNDING

This work was supported by National Science Foundation of Anhui Province (1808085MB47), Department of Education Committee of Anhui Province and the Center for Anhui Province Engineering of Modern Chinese Traditional Medicine (no. KJ2017A291), and the Opening Foundation of Anhui Province Key Laboratory of Environment-friendly Polymer Materials (no. 2018001).

SUPPLEMENTARY MATERIALS

Supplementary materials are available for this article at https://doi.org/10.1134/S1070328420110081 and are accessible for authorized users.

REFERENCES

1. Bajju, G.D., Devi, G., Ahmed, A., et al., *Russ. J. Inorg. Chem.*, 2019, vol. 64, p. 734. https://doi.org/10.1134/S0036023619060044
2. Pawlicki, M., Collins, H.A., Denning, R.G., et al., *Angew. Chem. Int. Ed.*, 2009, vol. 48, p. 3244.
3. Au, L., Zhang, Q., Cobley, C.M., et al., *ACS Nano*, 2010, vol. 4, p. 35.

4. Lermontova, S.A., Grigor'ev, I.S., Ladilina, E.Yu., et al., *Russ. J. Coord. Chem.*, 2018, vol. 44, p. 301. https://doi.org/10.1134/S1070328418040061
5. Zhang, H.R., Liu, Y.C., Chen, Z.F., et al., *Russ. J. Coord. Chem.*, 2018, vol. 44, p. 322. https://doi.org/10.1134/S107032841805007X
6. Jafari, M., Salehi, M., Kubicki, M., et al., *Russ. J. Coord. Chem.*, 2018, vol. 44, p. 21. https://doi.org/10.1134/S1070328418010086
7. Zhao, X.X., Liu, L.W., Li, Y.F., et al., *Russ. J. Coord. Chem.*, 2018, vol. 44, p. 439. https://doi.org/10.1134/S1070328418070060
8. Salehi, M., Galini, M., Kubicki, M., et al., *Russ. J. Inorg. Chem.*, 2019, vol. 64, p. 18. https://doi.org/10.1134/S0036023619010170
9. Padilha, L.A., Nootz, G., Olszak, P.D., et al., *Nano Lett.*, 2011, vol. 11, p. 1227.
10. Albota, M., Beljonne, D., Bredas, J.L., et al., *Science*, 1998, vol. 281, p. 1653.
11. Reinhardt, B.A., Brott, L.L., Clarson, S.J., et al., *Chem. Mater.*, 1998, vol. 10, p. 1863.
12. Chung, S.J., Kim, K.S., Lin, T.C., et al., *J. Phys. Chem., B*, 1999, vol. 103, p. 10741.
13. Luo, Y., Normal, P., Macak, P., et al., *J. Phys. Chem., A*, 2000, vol. 104, p. 4718.
14. Xu, G.Y., Wei, D., Wang, J.F., et al., *Dyes Pigments*, 2014, vol. 101, p. 312.
15. Norman, P., Luo, Y., and Agren, H., *J. Chem. Phys.*, 1999, vol. 111, p. 7758.
16. Macak, P., Luo, Y., Norman, P., et al., *J. Chem. Phys.*, 2000, vol. 113, p. 7055.
17. Li, D.M., Tian, X.H., Hu, G.J., et al., *Inorg. Chem.*, 2011, vol. 50, p. 7997.
18. Wang, X.C., Tian, X.H., Zhang, Q., et al., *Chem. Mater.*, 2012, vol. 24, p. 954.
19. Sneharani, A.H., Karakkat, J.V., Singh, S.A., et al., *J. Agric. Food. Chem.*, 2010, vol. 58, p. 11130.
20. Safavy, A., Raisch, KP., Mantena, S., et al., *J. Med. Chem.*, 2007, vol. 50, p. 6284.
21. Liu, K., Guo, T.L., Chojnacki, J., et al., *ACS Chem. Neurosci.*, 2012, vol. 3, p. 141.
22. Sheldrick, G.M., *SHELXS-97, Program for Crystal Structures*, Göttingen: Univ. of Göttingen, 1997.
23. Xu, G.Y., Wang, J.F., Si, G.F., et al., *Dyes Pigments*, 2015, vol. 123, p. 267.
24. Li, L., Tian, Y.P., Yang, J.X., et al., *Chem. Asian. J.*, 2009, vol. 4, p. 668.
25. Zhou, S.S., Xue, X., Wang, J.F., et al., *J. Mater. Chem.*, 2012, vol. 22, p. 22774.
26. Zhou, H.P., Li, D.M., Zhang, J.Z., et al., *Chem. Phys.*, 2006, vol. 322, p. 459.
27. Yan, Y.X., Tao, X.T., Sun, Y.H., et al., *J. Mater. Chem.*, 2004, vol. 14, p. 2995.